Surface & Coatings Technology 206 (2011) 378–386

Contents lists available at ScienceDirect

Surface & Coatings Technology

journal homepage: www.elsevier.com/locate/surfcoat

Microstructure and photocatalytic activity of suspension plasma sprayed TiO_2 coatings on steel and glass substrates

E. Bannier [a,*], G. Darut [b], E. Sánchez [a], A. Denoirjean [b], M.C. Bordes [a], M.D. Salvador [c], E. Rayón [c], H. Ageorges [b]

[a] Instituto de Tecnología Cerámica - Asociación de Investigación de las Industrias Cerámicas, Universitat Jaume I, Av. Vicent Sos Baynat s/n, 12006 Castellón, Spain
[b] SPCTS, UMR CNRS 6638, Université de Limoges, Faculté des Sciences et Techniques, 123 avenue Albert Thomas, 87060 Limoges, France
[c] Universidad Politécnica de Valencia, Instituto de Tecnología de Materiales, Camino de Vera s/n, 46022 Valencia, Spain

ARTICLE INFO

Article history:
Received 7 March 2011
Accepted in revised form 14 July 2011
Available online 23 July 2011

Keywords:
Photocatalytic coatings
Suspension plasma spraying
TiO_2
Microstructure

ABSTRACT

In this study, TiO_2 coatings were deposited by suspension plasma spraying (SPS) from a commercial TiO_2 nanoparticle suspension on two different substrates: a standard stainless steel and a Pyrex glass. Coatings were sprayed on both substrates with an F4-MB monocathode torch; a Triplex Pro tricathode torch was also used to spray coatings just on the stainless steel substrates. Spraying distance and cooling were varied.
The anatase content in the coatings, determined by XRD, ranged from 32 to 72 wt.%. A significant amount of anatase to rutile transformation was found to occur during cooling. Examination of the microstructure revealed that the coating microstructure was bimodal, involving a non-molten region consisting mainly of anatase nanoparticle agglomerates and a molten region. The glass substrate coatings displayed a segregated phase distribution, particularly when the surface to be coated was cooled. Photocatalytic activity was determined by a methylene blue test.
The experimental data fitted well to a first-order kinetic. All the coatings exhibited high photocatalytic activity in comparison with that of a commercial sol–gel coating. However, unlike much of the previous research, photocatalytic activity did not correlate with the anatase content determined by XRD.

1. Introduction

Nanostructured coatings are drawing increased scientific attention because of their potential enhancement of coating properties [1]. In conventional plasma spraying, micrometre-sized feedstock powders are injected within the plasma flow with a cold (i.e. room temperature) carrier gas. The decrease in particle size and weight from micro to nanoparticles requires an increase in particle injection velocity in order to keep the momentum quantity constant. As a result, the gas carrier flow rate also needs be raised, leading to disruption of the plasma and to untreated particles. Generally, two possible approaches can be used to manufacture nanostructured coatings: i) agglomeration of nanometre-sized particles into micrometre-sized feedstock that can be injected conventionally using a carrier gas or ii) use of a carrier liquid (suspension plasma spraying, SPS) instead of a carrier gas. SPS differs significantly from conventional atmospheric plasma spraying since the suspension is fragmented into droplets and the liquid phase vaporised before the solid feedstock is processed, leading to different interaction phenomena between plasma and particles, and to different thermal histories during spraying. The process has undergone extensive development, yielding nanostructured SOFC functional layers [2,3], thermal barrier coatings [4,5], wear resistant coatings [6], and photocatalytic layers [7]. Coatings with enhanced properties, in comparison with those of coatings obtained from conventional dry powders, have been reported [8].

Heterogeneous photocatalysis is a process that enables complete degradation of pollutants in water and air. Titanium dioxide (TiO_2) is, among semiconductors, the most widely used photocatalyst owing to its stability, non-toxicity, and relatively low cost.

Intense research in recent years has shown that thermal spray techniques, especially atmospheric plasma spraying (APS) and high velocity oxy-fuel spraying (HVOF), can be used to produce TiO_2 coatings with effective photocatalytic activity [9,10]. This, together with the inherent advantage of feeding nanoparticle suspensions instead of nanostructured powders into the plasma torch, as set out above, has further raised interest in the preparation of photocatalytic TiO_2 coatings by SPS [8,11].

A key issue throughout all this research has been the preservation of the largest possible quantity of anatase phase in the coating, because of the superior photocatalytical performance of anatase

* Corresponding author. Tel.: +34 964 64 24 24; fax: +34 964 34 24 25.
E-mail addresses: emilie.bannier@itc.uji.es (E. Bannier), geoffrey.darut@unilim.fr (G. Darut), enrique.sanchez@itc.uji.es (E. Sánchez), alain.denoirjean@unilim.fr (A. Denoirjean), carmen.bordes@itc.uji.es (M.C. Bordes), dsalva@mcm.upv.es (M.D. Salvador), emraen@upvnet.upv.es (E. Rayón), helene.ageorges@unilim.fr (H. Ageorges).

0257-8972/$ – see front matter © 2011 Elsevier B.V. All rights reserved.
doi:10.1016/j.surfcoat.2011.07.039

compared to that of rutile. In fact, numerous papers have demonstrated the need to achieve a minimum anatase content in the coating, correlating anatase content with photocatalytic activity [12–14]. However, controversy persists with regard to the factors that control TiO_2 phase (anatase versus rutile) distribution in the final layers. A mixture of anatase and rutile is always encountered, regardless of the nature and composition of the feedstock, while anatase and rutile contents can vary widely [15–17].

Toma et al. [18] recently showed that titania coatings obtained by SPS of aqueous suspensions led to better photocatalytic layers, stating that a minimum threshold of 15–20 vol.% anatase was needed to obtain significant pollutant degradation. A subsequent paper [19] reported that when the anatase ratio exceeded a maximum threshold of 65 vol.%, the anatase content contributed less to photocatalysis. Other factors could play a role such as those related to the adsorbed species on the coating surface [20].

Using submicrometric rutile suspensions, Kozerski et al. [21] recently showed that the photocatalytic performance of the titania deposits did not correlate with the anatase content, while coatings principally containing rutile were also photocatalytically active. That paper also noted the need for further research in order to clarify the relationship between process variables and coating microstructure in regard to photocatalytic activity.

The present study was undertaken to prepare photocatalytic TiO_2 coatings from aqueous nanoparticle suspensions by SPS. The impact of certain key plasma spraying conditions (such as spraying distance and cooling) on coating microstructure, phase distribution, and photocatalytic activity was studied. Standard stainless steel and Pyrex glass were used as substrates, the latter being tested in view of the growing interest in photocatalytic glass-supported coatings for wastewater treatment.

2. Materials and methods

2.1. Materials

All layers were deposited from a commercial suspension of TiO_2 nanoparticles (AERODISP 740X, Evonik Degussa GmbH, Germany). The main suspension characteristics, as given by the supplier, are listed in Table 1.

TEM observations (H7100, Hitachi, Japan) of the nanoparticles in this suspension confirmed their nanometre size (20–30 nm). XRD analysis (D8 Advance, Bruker) indicated that they contained 90 wt.% anatase and 10 wt.% rutile.

Stainless steel (AISI 304 grade) and Pyrex glass were used as substrates (25 mm diameter disks). The metal substrates were polished up to SiC 4000 and both types of samples were cleaned with ethanol before coating deposition.

2.2. Coating deposition

Coatings were deposited using two different plasma torches: an F4-MB monocathode torch (Sulzer Metco, Wolhen Switzerland) with a 6 mm internal diameter anode was used to coat both stainless steel and glass substrates, while a Triplex Pro tricathode torch (Sulzer Metco, Wolhen Switzerland) with a 6.5 mm diameter segmented anode was used to coat only steel substrates. The substrates were preheated (between 200 °C and 300 °C) to enhance coating adhesion.

Table 1
Nanosuspension main characteristics (according to supplier information).

Reference	Supplier	TiO_2 content (wt.%)	pH	Viscosity (mPa s)	Mean aggregate size (nm)	Density at 20 °C (g/cm^3)
Aerodisp 740 X	Evonik	40	5.0–7.0	<1000	<100	1.41

As can be observed in Fig. 1, samples were mounted on a rotating device and up to 6 samples were coated simultaneously. The suspensions were injected through a calibrated diaphragm of 150 μm average diameter. Suspension momentum density upon penetration in the plasma flow was controlled by adjusting the pressure in the suspension containers. The characteristics of the suspension feeding system have been described elsewhere [22]. For all coatings suspension feedrate was 23 ml min^{-1} (28.2 g min^{-1}).

The main spraying parameters used for each sample, as well as the sample references, are given in Table 2. All coatings were sprayed with a similar plasma mass enthalpy. The effects of both spraying distance and cooling were studied. Cooling was performed by spraying water (8 ml s^{-1}) with compressed air (1 bar) on the surface to be coated, throughout the process. During deposition, the samples temperature was measured using a pyrometer. As a consequence of the holder geometry (Fig. 1), the value measured using the pyrometer depends on both samples and holder temperatures. As holder and steel substrates display similar thermal conductivity, the temperature measured should be closed to the real sample temperature. However, in the case of glass samples, the temperature could not be determined accurately as a consequence of the important thermal conductivity differences existing between glass substrate and metallic holder.

For comparison purposes, a commercial photocatalytic TiO_2 sol–gel coating and three APS coatings were also deposited. The commercial sol–gel layer was obtained by spraying two suspensions on the substrate: a colloidal primer suspension (X-clean PK 3033 P, Nano-X GmbH, Germany) and a TiO_2 nanosuspension (X-clean PK 3033 F, Nano-X GmbH, Germany). After deposition the samples were thermally treated at 400 °C. The main spraying parameters used to deposit the APS coatings are given in Table 3. A complete characterization of the Al_2O_3–TiO_2 nanostructured coatings has been published elsewhere [23].

2.3. Determination of phase composition

The nanoparticles present in the suspension feedstock and the resulting coatings were tested by X-ray diffraction (XRD) analysis, in order to determine their crystalline phase compositions. Anatase content was quantified using the Rietveld method.

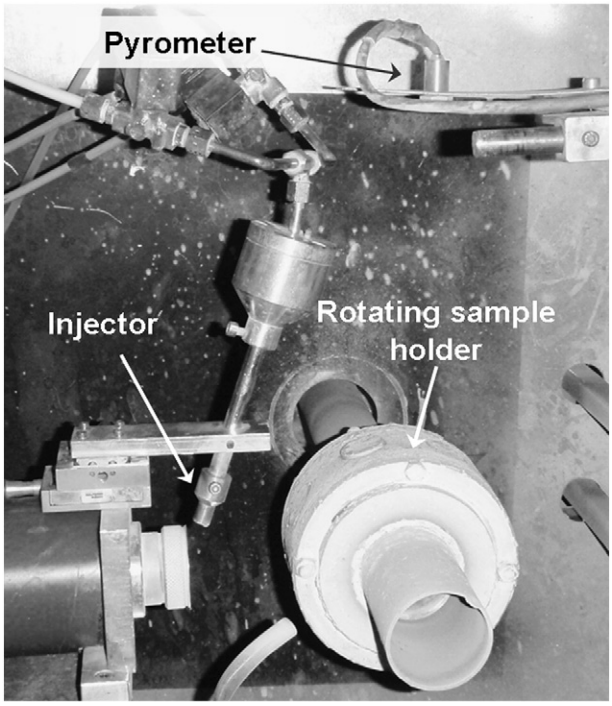

Fig. 1. Suspension plasma spraying equipment.

Table 2
Main spraying parameters and sample references.

Sample	Substrate	Torch	Nozzle (mm)	Ar (l/min)	He (l/min)	Arc intensity (A)	Arc tension (V)	Plasma mass enthalpy (MJ/kg)	Spray distance (mm)	Cooling
G1	Glass	F4-MB	6	50	10	400	39	5.7	60	No
G2	Glass	F4-MB	6	50	10	400	38	5.7	40	No
G3	Glass	F4-MB	6	50	10	400	39	5.8	40	Yes
G4	Glass	F4-MB	6	50	10	400	39	5.8	50	Yes
G5	Glass	F4-MB	6	50	10	400	39	5.7	50	No
S1	Steel	F4-MB	6	50	10	400	39	5.4	40	No
S2	Steel	F4-MB	6	50	10	400	39	5.6	60	No
S3	Steel	F4-MB	6	50	10	400	39	5.5	50	No
S4	Steel	F4-MB	6	50	10	400	38	5.6	50	Yes
ST1	Steel	Triplex Pro	6.5	60	0	200	80	5.8	60	No
ST2	Steel	Triplex Pro	6.5	60	0	200	80	5.8	40	No

Table 3
APS spraying parameters.

Coating	Powder reference	Powder supplier	Torch	Nozzle (mm)	Ar (l/min)	He (l/min)	H_2 (l/min)	Arc intensity (A)	Spray distance (mm)
APS-Al_2O_3 (conventional)	METCO 105 SFP	Sulzer Metco, Germany	F4-MB	6	35	–	12	600	120
APS-(Al_2O_3–13wt.%TiO_2) (nanostructured)	NANOX S2613S	Inframat advanced Materials, USA	F4-MB	6	35	–	12	600	120
APS-TiO_2 (nanostructured)	NEOXID T101 nano	MilliDyn, Finland	F4-MB	6	40	20	–	600	120

The XRD diffractograms were obtained using a Bruker Theta–Theta model D8 Advance diffractometer with CuKα radiation (λ = 1.54183 Å). The generator settings were 45 kV and 30 mA. The XRD data were collected in a 2θ range of 5–90° with a step width of 0.015° and a counting time of 1.2 s/step. A VÅNTEC-1 detector was used.

In the case of the feeding nanoparticles, powder samples were prepared by drying the suspension feedstock and milling the resulting material in a pneumatic tungsten carbide ring mill to obtain agglomerates size below 40 μm [24]. The milled powder was subsequently backfilled into an appropriate specimen holder.

A quantitative phase analysis was conducted [25,26] and the collected data were used in a Rietveld refinement [27,28]. The 4.2 version of the DIFFRACplus TOPAS Rietveld analysis program was used in this study, assuming a pseudo-Voight function to describe peak shapes. The refinement protocol included the background, scale factors, and instrument, as well as the sample lattice, profile, and texture parameters. The basic approach consists, first, of identifying all the crystalline phases present in the sample and then inputting the corresponding basic structural data. Finally, computer modelling is used to find the best fit to experimental patterns. An internal standard (fluorite) with a known concentration was introduced to analyse the powder samples. Rwp (R-weighted pattern) and GOF (goodness-of-fit) parameters were calculated in order to evaluate the accuracy of results.

2.4. Observation of microstructure

Coating microstructure was investigated by scanning electron microscopy (SEM) using an FEI Quanta 200F field-emission gun-SEM, connected to an energy-dispersive X-ray microanalysis (EDX) instrument. SEM observations were performed on polished cross-sections of the different samples.

A HORIBA Jobin Yvon Raman spectrometer configured at 514.5 nm emission was used to characterise some coated sample cross-sections. The localisation of the analysis spot of the argon-ion laser was driven by an optical microscope.

2.5. Characterisation of photocatalytic activity

The photocatalytic activity of the coatings was ascertained by studying the decomposition of a 5 ppm methylene blue (MB) aqueous solution under UV radiation. Irradiation was performed in a chamber using a UV-lamp (λ = 370 nm) with an intensity of 2.5 mW/cm^2. The coated samples (25 mm diameter disks) were immersed in a glass beaker containing 25 ml of MB solution. MB solution absorbance was measured at 664 nm wavelength, which is the maximum absorption peak of MB, using a UV–visible spectrometer (Spectro SC, Labomed Inc., USA). In order to allow the MB to be adsorbed on to the TiO_2 surface, the test pieces were kept in contact with the solution for 30 min in the dark, after which the MB concentration was determined. Afterwards, the samples were continuously irradiated, a 6 ml volume being withdrawn after 1, 2, 3, 5, 7, and 11 h of irradiation to determine the concentration. The solution was stirred before each sampling and the withdrawn test liquid was returned to the solution after UV measurement. A blank sample with no coating was tested to evaluate the influence of UV radiation on the decrease in MB concentration by photolysis.

3. Results and discussion

3.1. Sample temperature during deposition

Fig. 2 gives the evolution of the temperature during spraying of samples S1, S3 and S4. First, substrates were pre-heated using the plasma torch. When the temperature reaches about 300 °C, the aqueous suspension was introduced leading to a significant drop in both plasma and sample temperatures. For selected spray conditions, the cooling was also turned on at the end of the pre-heating period.

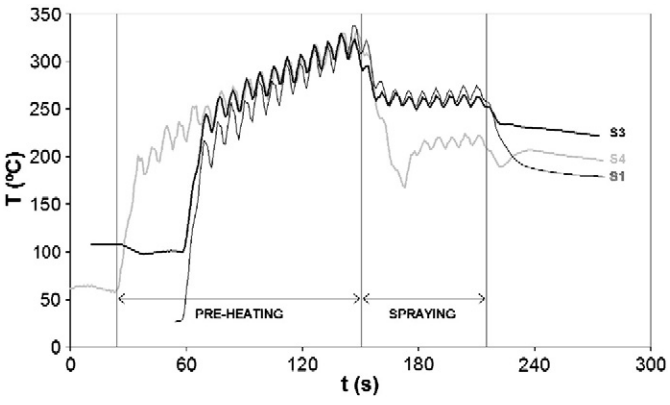

Fig. 2. Evolution of the samples temperature during spraying.

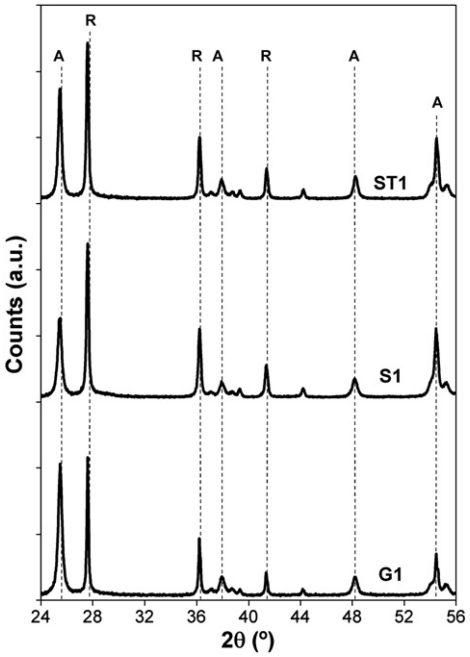

Fig. 3. XRD patterns of coatings G1, S1, and ST1. The peaks labelled A and R correspond, respectively, to anatase and rutile phases.

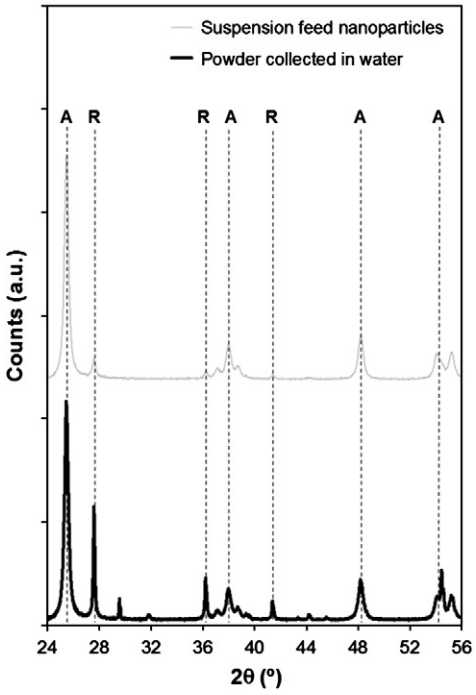

Fig. 4. XRD patterns of the suspension feedstock nanoparticles (top) and of the in-flight particles collected in water (bottom). The peaks labelled A and R correspond, respectively, to anatase and rutile phases.

It can be observed that sample temperature is only slightly dependent on the spraying distance, whereas cooling leads to significantly lower temperature values during deposition.

3.2. Composition of the crystalline phases

3.2.1. Anatase content

XRD analysis along with Rietveld refinement revealed that all deposited coatings consisted of mixtures of rutile and anatase (Fig. 3). It was found that the coatings contained between 32 and 72 wt.% anatase (Table 4). Moreover, suspension feedstock was sprayed with an F4-MB torch and the in-flight particles were collected in water instead of being allowed to impinge upon the substrate. The resulting powder was dried and analysed by XRD, showing an anatase content of 74 wt.% whereas the feedstock initially contains 90 wt.% anatase (Table 4, Fig. 4).

From the phase composition analysis, the following results may be highlighted:

- The anatase content was lower in the coatings than in the initial suspension, which indicates phase transformation of titanium dioxide during deposition.
- In-flight particles display lower rutile content than the coatings, as a consequence it may be assumed that much of the phase transformation occurred after particle deposition.
- Cooling led to notably higher anatase content (Fig. 5).
- Spraying distance had a major effect on coating crystalline phase composition: anatase content increased significantly with spraying distance (Fig. 6).
- The type of plasma torch affected the crystalline phase composition. At similar spraying distance and plasma enthalpy, the layers deposited with the tricathode gun displayed lower anatase content (Fig. 6).
- Substrate nature had no notable influence on the phase composition (Fig. 6).

Table 4
Feedstock and coating characteristics.

Sample	Thickness (μm)	Anatase (wt.%)	Rutile (wt.%)	Rietveld refinement	
				Rwp	GOF
Suspension feedstock	–	90	10	9.30	1.55
In-flight particles	–	74	26	9.98	1.78
G1	15	59	41	15.68	2.52
G2	29	38	62	11.18	1.82
G3	28	69	31	14.43	2.43
G4	15	72	28	16.83	2.75
G5	39	46	54	11.50	1.87
S1	45	37	63	10.61	1.73
S2	23	59	41	14.15	2.49
S3	32	46	54	10.70	1.70
S4	14	68	32	15.52	2.95
ST1	36	44	56	9.85	1.60
ST2	55	32	68	11.24	1.76

3.2.2. Anatase to rutile phase transformation mechanisms

In order to obtain coatings with large amount of anatase, it is generally considered that the plasma plume temperature must be low

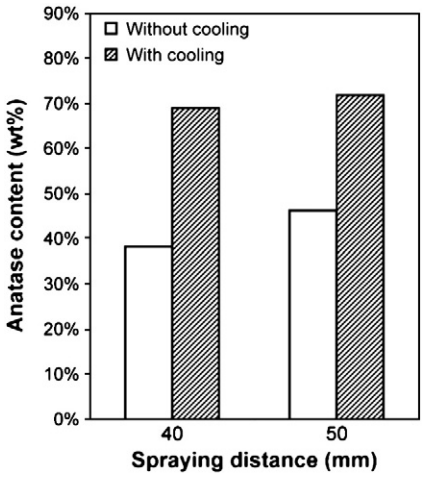

Fig. 5. Effect of cooling on coating anatase content (glass substrate).

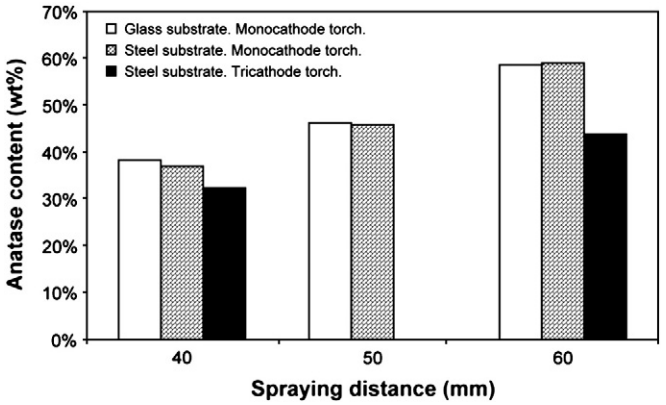

Fig. 6. Effect of spraying distance on coating anatase content (glass and steel substrates, without cooling).

enough to avoid an excessive particles heating, which will promote the phase transformation [29]. Indeed, it is commonly accepted that transformation from anatase to rutile occurs at a temperature of about 900 K [30].

Actually, the anatase found in the coatings may come from unmolten particles, which retained the initial powder crystalline structure [20], or from the nucleation of anatase from melted particles [31], which explained that some anatase is found even when the suspension feedstock is purely rutile [16,21]. After impingement of the molten particles onto the substrate, the anatase to rutile transformation is promoted by the reheating of previously deposited layers by successive passes of the torch [32].

In fact, from a thermodynamics point of view the recrystallisation of anatase from the liquid phase is more favourable, due to its lower surface energy compared to rutile [30]. Then, anatase will transform to rutile, which displays a lower Gibbs free-energy. However, the anatase to rutile transformation is reconstructive, which means that it is time dependent [30]. As a consequence, a higher cooling rate of the coatings after deposition should reduce the formation of rutile, which is confirmed by the results shown in Table 4: the coatings obtained using water cooling (samples G3, G4, and S4) yielded the highest anatase content.

It was also found that using the tricathode torch leads to lower anatase content (Table 4). In fact, the tricathode torch led to more efficient heat transfer from the plasma to the particles and, though, to enhanced particle heating inside the plasma jet. As the particles reach higher temperature, the driving force for anatase to rutile transformation is increased leading to higher rutile content in the coating.

Several authors have reported that spraying distance has a significant effect on anatase content [16,31]. The results obtained in this study confirmed that the quantity of anatase to rutile transformation decreased when the plasma torch was moved farther from the sample (Table 4). As the temperature of the samples is not significantly influenced by the spraying distance (Fig. 2), it may be assumed that the differences found in the crystalline structure are not mainly due to changes in the cooling rate. Yet several hypotheses may explain these results. First, spraying distance may influence the particles velocity, leading to differences in splat flattening. Actually, Colmenares-Angulo et al. have shown that at higher impact velocity, the anatase content increased due to an enhancement in splat flattening and, though, to higher splat solidification rate [32]. As a result, the amount of anatase to rutile transformation is reduced. Furthermore, Jaworski et al. have reported that, as spraying distance augments, the number of particles which resolidify before impact onto the substrate is increased [31]. The entrapment of such particles inside the coatings might promote the formation of a higher amount of rutile [32]. Finally, as the spraying distance is increased, the flight time in the plasma jet is longer, which gives more time for the anatase to rutile transformation to occur before impact on the substrate.

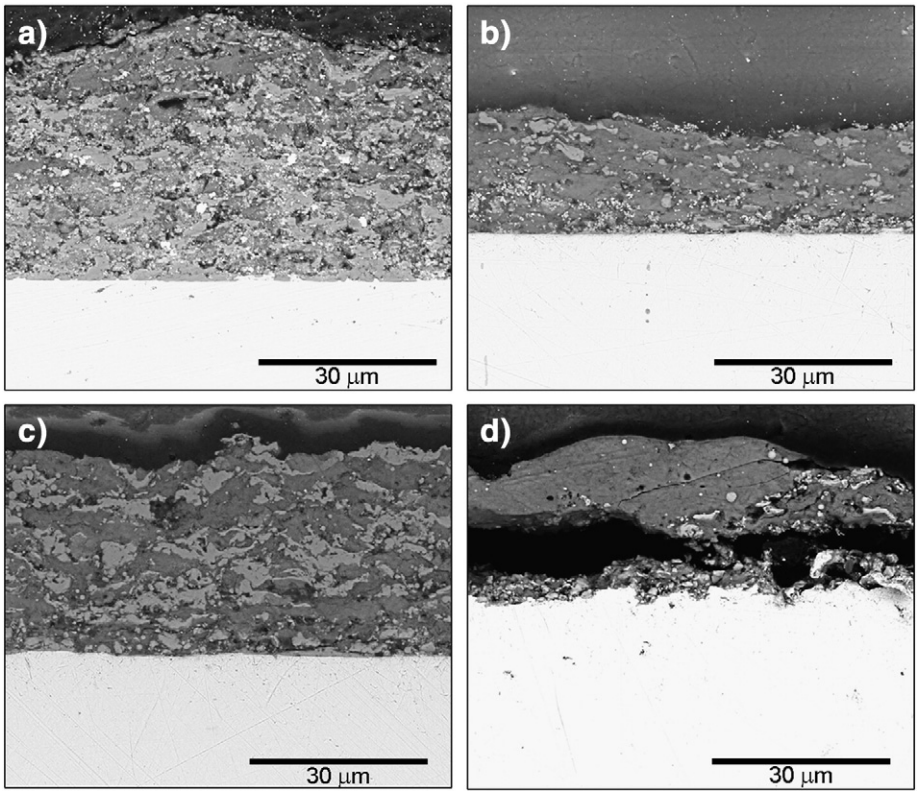

Fig. 7. SEM micrographs of suspension plasma sprayed TiO_2 coatings obtained on steel substrates with an F4-MB plasma gun: a) S1, b) S2, c) S3, and d) S4.

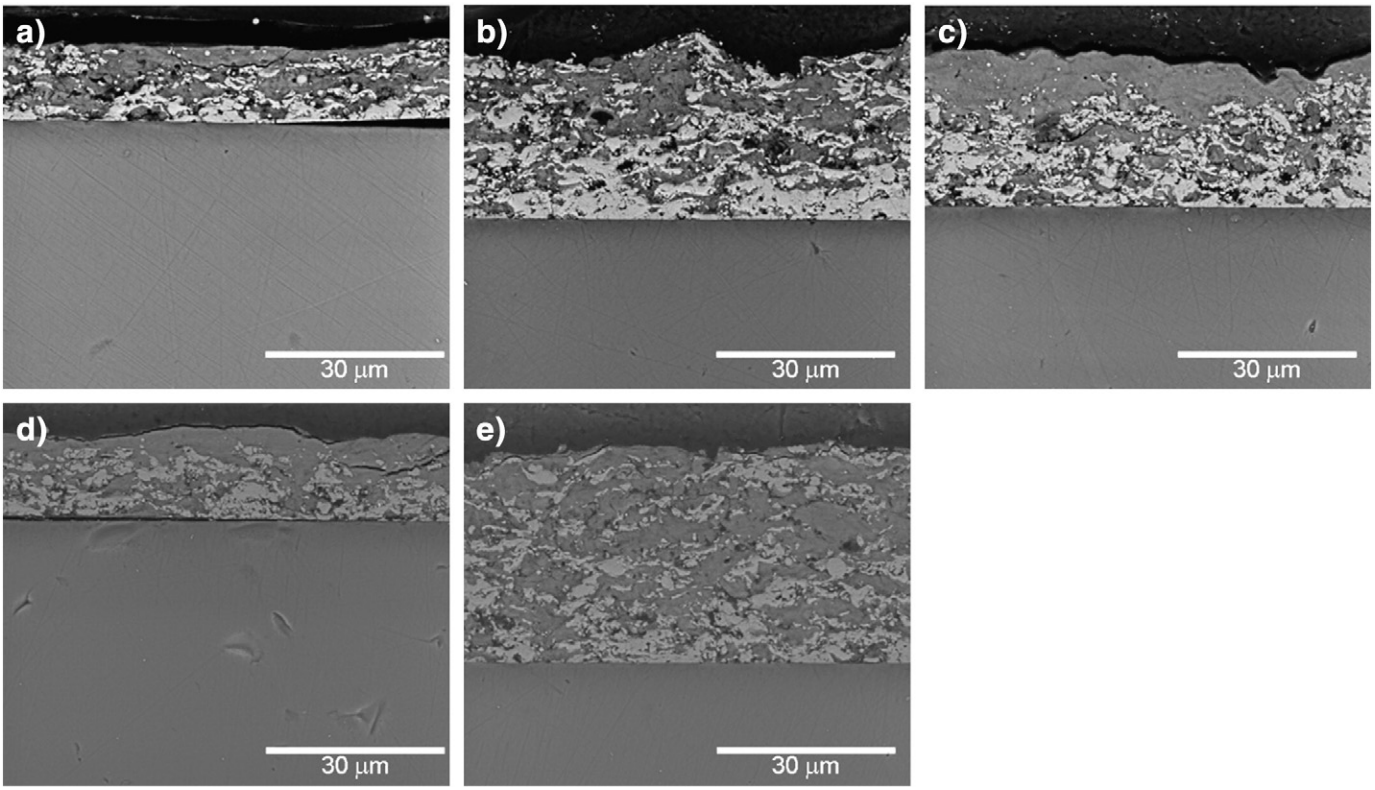

Fig. 8. SEM micrographs of suspension plasma sprayed TiO_2 coatings obtained on glass substrates with an F4-MB plasma gun: a) G1, b) G2, c) G3, d) G4, and e) G5.

3.3. Coating microstructure

Coating microstructure was observed by SEM (Figs. 7 to 10). All coatings were dense and the porosity measurable by optical or electronic microscopy was negligible. In general, the coatings consisted of a bimodal microstructure characterised by the presence of completely fused (light-coloured) regions and of non-molten (dark-coloured) regions consisting of agglomerated nanoparticles, as may be observed in the high-magnification micrographs (Fig. 10). Such microstructures, characterised by a distribution of non-melted and melted regions, have been previously reported in suspension plasma sprayed coatings obtained from titania and other materials such as alumina [18]. The microstructure develops because, when the suspension is injected into the plasma, the drops generated by the continuous jet break-up are accelerated in the plasma and disintegrated into smaller ones. At the same time, the water still present in the droplets boils and evaporates: the resulting particles may thus be heated, partly melted, or melted, yielding the end coating. The resulting microstructure largely depends on the characteristics of the suspension feedstock and the plasma feed system [21,29].

Anatase content determined by XRD seems to increase when the total area of non-molten regions augments. As a consequence, anatase phase is expected to occur mostly in the non-molten areas. However, part of the anatase may have crystallised from liquid droplets and may, therefore, belong to the molten areas, as set out above [16,32].

In the case of the steel substrate coatings, molten and non-molten areas were quite intimately mixed. In contrast, segregation was observed in the glass substrate coatings, which led to an increase in the non-molten areas from the deposit–substrate interface upward to the outer deposit surface. This effect was particularly notable on cooled glass substrate (coatings G3 and G4 in Fig. 8), suggesting that a higher cooling rate promotes the segregation. However, as samples G1 and G2 presented the same type of microstructure, cooling is not the only factor of influence. Further investigation will be needed in order to fully understand the origin of the segregation.

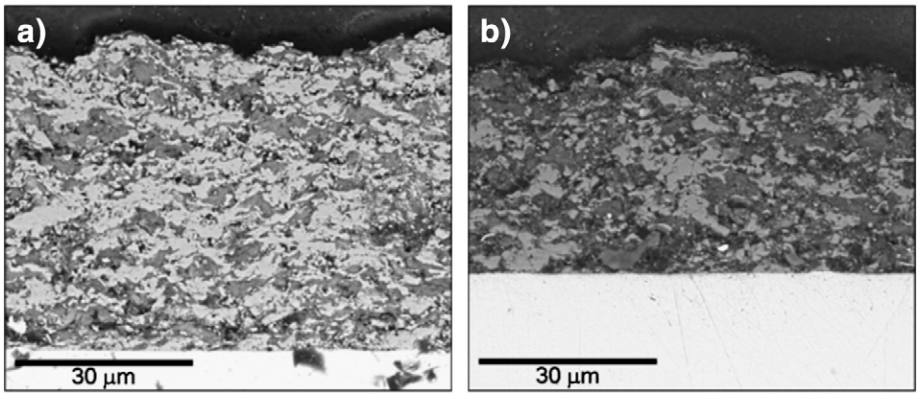

Fig. 9. SEM micrographs of suspension plasma sprayed TiO_2 coatings obtained on steel substrates with a Triplex Pro torch: a) ST2 and b) ST1.

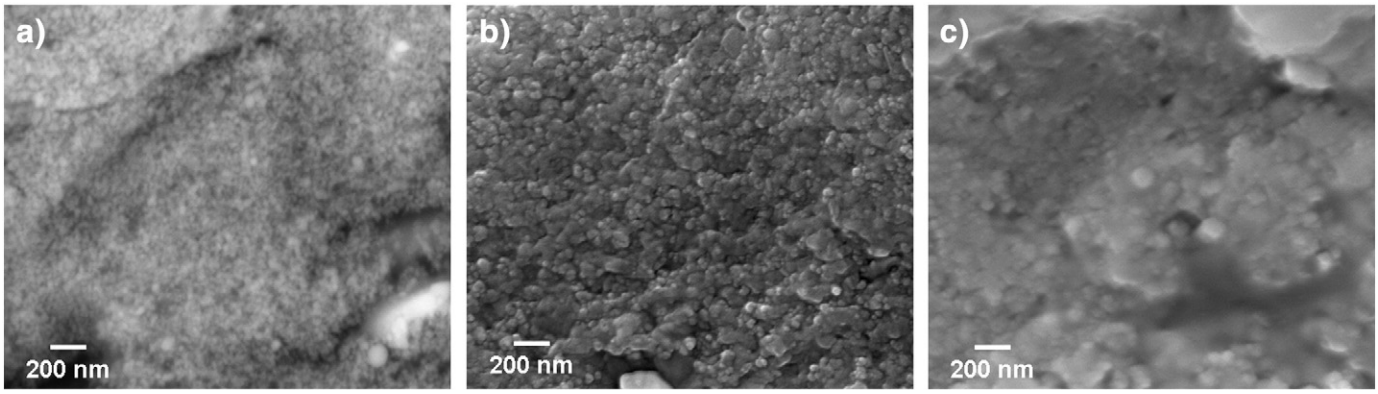

Fig. 10. High-magnification SEM micrographs (×120,000) of non-molten areas found in the coatings: a) G2, b) S2, and c) ST2.

Finally, cooling usually resulted in degradation of the microstructure, leading to poorer adhesion and the presence of many defects, such as cracks. Such problems presumably stemmed from the presence of a water film on the sample surface, which hindered particle deposition. As a result of differences in the holding systems used for the glass and steel substrates, the water film was much thicker in the case of the steel substrates, which probably explains the poor quality of coating S4 (Fig. 7d). Finally, significant differences were noted in coating thickness (Table 4). In particular, on steel substrate the coating thickness increased when the spraying distance decreased and/or when the tricathode torch was used, probably owing to higher spraying efficiency.

In order to properly identify whether the anatase phase was particularly associated with the non-melted areas, a Raman microscopy analysis was performed on selected coating samples. The technique has already been successfully used in discerning anatase and rutile phases in the microstructure of titania coatings [16]. The analysis was carried out on the G3 sample, which displayed clearly segregated non-molten and molten areas, owing to water cooling of the glass substrate surface to be coated. The microstructure of this coating, together with the spot size of the Raman laser on each (molten and non-molten) region, is depicted in Fig. 11. The Raman curves show that the non-molten region located in the surface of sample G3 consisted entirely of anatase, while the XRD results for this sample showed that it contained 69% anatase. It may be noted that the XRD technique, which is carried out at the surface, penetrates several tens of micrometres (approximately 20 μm for TiO_2 coatings) into the coating layer, whereas Raman spectroscopy focuses on spots a few micrometres in size in the sample cross-section. As a result, the findings cannot be compared.

3.4. Photocatalytic activity

Coating photocatalytic activity was determined by measuring the degradation of methylene blue (MB) dye in an aqueous solution. The variation in MB with irradiation time for the solutions in contact with sample G1 and with a blank substrate (B) is shown in Fig. 12.

Clear differences were found in the solution concentrations at each irradiation time. A pronounced decrease in concentration was observed for the coated sample, whereas the blank substrate exhibited no significant degradation after the UV irradiation. This finding verified the photocatalytic activity of the test coating. Similar results were obtained for all coatings sprayed on to both glass and steel substrates, independently of the type of plasma torch used. In addition, MB initial adsorption at the end of soaking time in the dark was quite small in every case, confirming the low porosity found in the coatings.

The variation in MB concentration with time may be represented using the Langmuir–Hinshelwood first-order kinetic equation, which is applied to low concentrations [33]:

$$-\frac{dC}{dt} = k'C. \tag{1}$$

After integration, Eq. (1) gives:

$$-\ln\frac{C}{C_0} = k't \tag{2}$$

where C is the MB concentration (ppm), C_0 is the MB initial concentration after residence time in darkness (ppm), t is the irradiation time (h), and k' is the constant of photocatalytic activity (h^{-1}). The plot of $\ln(C_0/C)$ versus time yields a straight line whose slope corresponds to the rate constant k'. Fig. 13 shows the variation of $\ln(C_0/C)$ with irradiation time for sample G1. A higher value of k' means a faster degradation rate of the organic molecule.

The rate constants and correlation coefficients (r^2) determined from the kinetic model (Eq. (2)) for all coatings are presented in

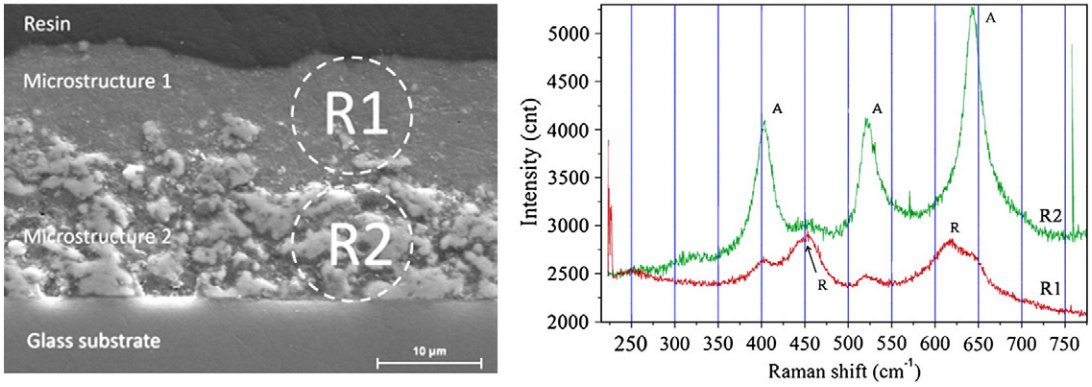

Fig. 11. Raman spectra results in the marked sites (R1 and R2 spots) of sample G3. A: Anatase and R: Rutile.

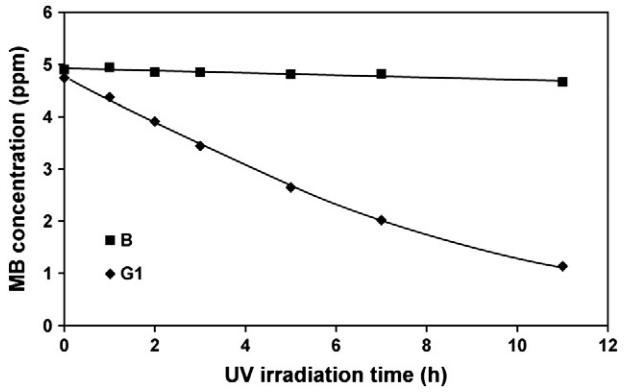

Fig. 12. Variation of MB concentration with UV irradiation time for solutions in contact with the G1 coating and with a blank sample.

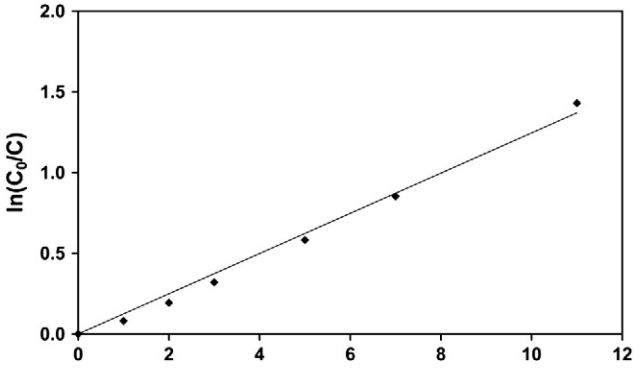

Fig. 13. Variation of $\ln(C_0/C)$ with irradiation time for sample G1.

Table 5. In each case, the correlation coefficients were higher than 0.988, indicating a reasonably good fit of the kinetic model to the experimental data. A similar fit was found by Toma et al. [18] with suspension plasma sprayed titania coatings, though the rate constants were quite different owing to the different test conditions and chemical reagent used.

For comparison purposes, the k' values were determined in the case of a commercial photocatalytic TiO_2 sol–gel coating and of 3 atmospheric plasma sprayed coatings (Al_2O_3, Al_2O_3–13 wt.%TiO_2 and TiO_2). The k' values detailed in Table 6 show that the photocatalytic activity of the suspension plasma sprayed coatings prepared in this study was almost twice that of the titania coating obtained from the dry powder, and even much higher than that of the commercial sol–gel coating. These results confirm the good photocatalytic performance of the suspension plasma sprayed TiO_2 coatings.

The value of k' versus anatase content of all the test coatings is plotted in Fig. 14. Unlike most previous research, no correlation was

Table 5
Photocatalytic rate constants and correlation coefficients of the coatings.

Sample	Rate constant (10^{-2} h^{-1})	r^2
G1	12.5	0.991
G2	13.2	0.989
G3	15.0	0.990
G4	11.8	0.998
G5	12.2	0.988
S1	15.0	0.992
S2	11.2	0.990
S3	13.7	0.992
S4	14.0	0.990
ST1	13.5	0.991
ST2	17.1	0.989

Table 6
Photocatalytic rate constants of three APS coatings and one commercial sol–gel coating, obtained elsewhere by the authors.

Sample	Rate constant (10^{-2} h^{-1})
APS-Al_2O_3	0.5
APS-(Al_2O_3–13wt.%TiO_2)	2.4
APS-TiO_2	7.3
Commercial TiO_2 sol–gel	5.8

observed between both variables. However, this finding was to some extent expected since, as indicated above, the amount of anatase phase determined by XRD did not suitably represent the amount of anatase phase at the coating surface. The lack of linear correlation between anatase content and photocatalytic activity was already reported by Toma et al. [19]. These authors demonstrated the need to consider other factors, such as coating surface hydroxylation, the amount and binding strength of the bonded water, or other adsorbed species on the coating surface, in order to explain the photocatalytic activity of suspension plasma sprayed coatings with high anatase content. Kozerski et al. [21] recently confirmed this lack of correlation and demonstrated the photocatalytic activity of suspension plasma sprayed titania coatings that consisted mainly of rutile. All these results underline the role of the surface in photocatalytic activity and the need, therefore, to physically and chemically analyse the coating surface and the interaction between the surface and the environment. Different coatings are currently being analysed by IR and XPS with a view to better understanding this issue.

4. Conclusions

TiO_2 coatings were prepared by suspension plasma spraying from a commercial TiO_2 nanoparticle suspension using two different substrates (a standard stainless steel and a Pyrex glass), modifying spraying distance, cooling, and type of plasma-torch.

A large amount of anatase was obtained, ranging from 32 to 72 wt.%. The nature of the substrate was found to have no notable influence on anatase content. In contrast, the type of plasma torch significantly affected the resulting amount of anatase. Spraying distance, as well as cooling, had a major effect on coating crystalline phase composition: anatase content increased significantly with both cooling and spraying distance.

In general, the resulting coatings displayed a bimodal microstructure characterised by the presence of completely fused regions, as well as of non-molten regions comprising agglomerated anatase nanoparticles. The anatase phase was mostly found in the non-molten areas. In the coatings sprayed on steel substrates, the molten and non-molten areas were quite intimately mixed, whereas segregation was

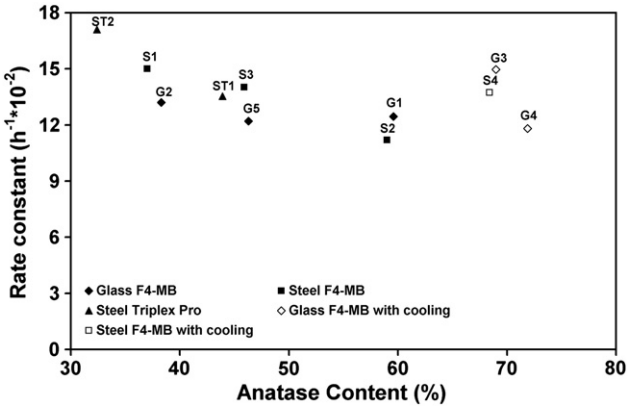

Fig. 14. Effect of anatase content (wt.%) on coating photocatalytic activity.

observed in the case of the glass substrate coatings, particularly when the glass surface to be coated was cooled.

Coating photocatalytic activity was determined by measuring the degradation of methylene blue (MB) dye in an aqueous solution. The studied first-order kinetic model exhibited a reasonably good fit to the experimental data for all test coatings. The values of the kinetic constant for these coatings were, in every case, much higher than that for a commercial sol–gel coating. However, unlike most previous research, photocatalytic activity was not observed to correlate with the anatase content determined by XRD.

Acknowledgements

This work has been supported by the Spanish Ministry of Science and Education (MAT2009-14144-C03-01), by the Spanish Ministry of Science and Innovation (PID-600200-2009-5) and by the European Commission in the frame of the Interreg IV B Sudoe programme (Eliare: SOE1/P1/F169).

References

[1] M. Gell, Mater. Sci. Eng. A 204 (1995) 246.
[2] P. Fauchais, R. Etchard-Salas, C. Delbos, M. Tognonvi, V. Rat, J.F. Coudert, T. Chartier, J. Phys. D Appl. Phys. 40 (2007) 2394.
[3] D. Waldbilig, O. Kesier, Z. Tang, A. Burgess, in: B.R. Marple, et al., (Eds.), Thermal Spray: Global Coating Solutions, ASM International, Materials Park [OH], 2007, p. 677.
[4] A.D. Jadhav, N.P. Padture, Surf. Coat. Technol. 202 (2008) 4976.
[5] J. Oberste-Berghaus, J.G. Legoux, C. Moreau, J. Therm. Spray Technol. 17 (2008) 91.
[6] J. Oberste-Berghaus, B.R. Marple, C. Moreau, J. Therm. Spray Technol. 15 (2006) 676.
[7] L. Pawlowski, Surf. Coat. Technol. 202 (2008) 4318.
[8] L. Pawlowski, Surf. Coat. Technol. 203 (2009) 2807.
[9] Zeng Yi, Wu. Juntao Li, Jianrong Wang Wei, Soo Wohn Lee, Ceram. Int. 34 (2008) 351.
[10] G. Bolelli, V. Cannillo, R. Gadow, A. Killinger, L. Lusvarghi, J. Rauch, Surf. Coat. Technol. 203 (2009) 1722.
[11] F.-L. Toma, G. Bertrand, D. Klein, C. Meunier, S. Begin, J. Nanomater. (2008) http://www.hindawi.com/journals/jnm/2008/384171.html [Visited: 2010-12-02].
[12] F.-L. Toma, D. Sokolov, G. Bertrand, D. Klein, C. Coddet, C. Meunier, J. Therm. Spray Technol. 15 (2006) 576.
[13] X.Y. Wang, Z. Liu, H. Liao, D. Klein, C. Coddet, Thin Solid Films 451–452 (2004) 37.
[14] L. Toma, N. Keller, G. Bertrand, D. Klein, C. Coddet, Int. J. Photoenergy 5 (2003) 141.
[15] J. Colmenares-Angulo, S. Zhao, C. Young, A. Orlov, Surf. Coat. Technol. 204 (2009) 423.
[16] H. Podlesak, L. Pawlowski, J. Laureyns, T. Jaworski, T. Lampke, Surf. Coat. Technol. 202 (2008) 3723.
[17] E. Bemporad, G. Bolelli, V. Cannillo, D. de Felicis, R. Gadow, A. Killinger, L. Lusvarghi, J. Rauch, M. Sebastiani, Surf. Coat. Technol. 204 (2010) 3902.
[18] F.-L. Toma, L.-M. Berger, C.C. Stahr, T. Naumann, S. Langner, J. Therm. Spray Technol. 19 (2010) 262.
[19] F.-L. Toma, L.-M. Berger, D. Jacquet, D. Wicky, I. Villaluenga, Y.R. de Miguel, J.S. Lindeløv, Surf. Coat. Technol. 203 (2009) 2150.
[20] F.-L. Toma, G. Bertrand, S. Begin, C. Meunier, O. Barres, D. Klein, C. Coddet, Appl. Catal. B Environ. 68 (2006) 74.
[21] S. Kozerski, F.-L. Toma, L. Pawlowski, B. Leupolt, L. Latka, L.-M. Berger, Surf. Coat. Technol. 205 (4) (2010) 980.
[22] R. Etchart-Salas, V. Rat, J.F. Coudert, P. Fauchais, N. Caron, K. Wittmann Teneze, S. Alexandre, J. Therm. Spray Technol. 16 (5–6) (2007) 857.
[23] E. Sánchez, E. Bannier, M. Vicent, A. Moreno, M.D. Salvador, V. Bonache, E. Klyatskina, A.R. Boccaccini, Int. J. Appl. Ceram. Technol. (2010), doi:10.1111/j.1744-7402.2010.02547.x.
[24] E. Burkhe, R. Jenkins, D.K. Smith (Eds.), A Practical Guide for the Preparation of Specimens for X-ray Fluorescence and X-ray Diffraction Analysis, Wiley, New York, 1998, p. 171.
[25] A.L. Ortiz, F. Sánchez-Bajo, F.L. Cumbrera, F. Guiverteau, Mater. Lett. 49 (2001) 137.
[26] A.L. Ortiz, F. Sánchez-Bajo, N.P. Padture, F.L. Cumbrera, F. Guiverteau, J. Eur. Ceram. Soc. 21 (2001) 1237.
[27] R.E. Young (Ed.), The Rietveld Method, University press, Oxford, 1996.
[28] H.M. Rietveld, J. Appl. Crystallogr. 2 (1969) 65.
[29] F.L. Toma, G. Bertrand, D. Klein, C. Coddet, C. Meunier, J. Therm. Spray Technol. 15 (2006) 587.
[30] D.A.H. Hanaor, C.C. Sorrell, J. Mater. Sci. 46 (2011) 855.
[31] R. Jaworski, L. Pawlowski, F. Roudet, S. Kozerski, A. le Maguer, J. Therm. Spray Technol. 17 (2008) 73.
[32] J.R. Colmenares-Angulo, V. Cannillo, L. Lusvarghi, A. Sola, S. Sampath, J. Mater. Sci. 44 (2009) 2276.
[33] A. Houas, H. Lachleb, M. Ksibi, E. Elaloui, C. Guillard, J.M. Herrmann, Appl. Cat. B Environ. 31 (2001) 145.